Application of a high-repetition-rate laser diagnostic system for single-cycle-resolved imaging in internal combustion engines

Johan Hult, Mattias Richter, Jenny Nygren, Marcus Aldén, Anders Hultqvist, Magnus Christensen, and Bengt Johansson

High-repetition-rate laser-induced fluorescence measurements of fuel and OH concentrations in internal combustion engines are demonstrated. Series of as many as eight fluorescence images, with a temporal resolution ranging from 10 μs to 1 ms, are acquired within one engine cycle. A multiple-laser system in combination with a multiple-CCD camera is used for cycle-resolved imaging in spark-ignition, direct-injection stratified-charge, and homogeneous-charge compression-ignition engines. The recorded data reveal unique information on cycle-to-cycle variations in fuel transport and combustion. Moreover, the imaging system in combination with a scanning mirror is used to perform instantaneous three-dimensional fuel-concentration measurements.

OCIS codes: 120.1740, 300.2530.

1. Introduction

The fuel–air mixing and combustion processes within the cylinder of an internal combustion (IC) engine to a large extent determine the engine efficiency and emissions. Simulations of the two processes can be performed by use of computational fluid dynamics, but the current precision of this tool makes in-cylinder diagnostics necessary to fully understand fuel–air mixing and combustion. Two types of optical techniques exist. The older is direct imaging of fuel sprays or combustion processes by use of line-of-sight integrating techniques. High-speed imaging of flame propagation at 10 kHz or more has been performed since the 1930's,[1] and the same technique can also be applied to visualize fuel-spray penetration. The problem with direct imaging is that only the outer surface of a flame or spray can be imaged. This means that the processes within a flame kernel or spray remain unknown. Laser diagnostics can be used to reveal the internal structure of flames and sprays.[2] By forming the laser beam into a two-dimensional (2-D) sheet and using a 2-D detector such as a CCD camera, one can get an image of a cross section through a flame or spray at a given time. Normally, a pulsed laser is used to get high power density in the sheet and thus a good signal-to-noise ratio. However, this limits the repetition rate of the experiments. Most Nd:YAG lasers are limited to a 10–50-Hz repetition rate, and excimer lasers are only marginally faster. The limited repetition rate means that only one image can be obtained per engine cycle. Cu^{+} lasers have repetition rates of as high as 50 kHz, but the low pulse energy allows them to be used only for Mie scattering experiments. To follow spray or flame propagation, one must use many cycles, and statistical material is captured for each crank angle. If only the mean spray penetration or flame behavior is of interest, the limitation of one image per cycle can be accepted, but if the stability of the process is low, the single-image technique suffers significantly. One process with low stability is the early flame development in a spark-ignition (SI) engine. The early flame grows and moves quite differently from cycle to cycle. The average flame growth obtained from single-shoot measurements can here differ more than a factor of two from that measured on a cycle-to-cycle basis.

High-repetition-rate laser diagnostics allow single-cycle-resolved engine measurements, in which single

J. Hult (johan.hult@forbrf.lth.se), M. Richter, J. Nygren, and M. Aldén are with the Department of Combustion Physics, Lund Institute of Technology, P.O. Box 118, SE-22100, Lund, Sweden. A. Hultqvist, M. Christensen, and B. Johansson are with the Department of Combustion Engines, Lund Institute of Technology.

Received 26 October 2001; revised manuscript received 25 April 2002.

0003-6935/02/245002-13$15.00/0

combustion events can be followed in time. Cycle-to-cycle variations of complex events can be studied, which is impossible from single-shot images captured in different cycles. As individual structures can be followed in time, the large-scale development of, e.g., a spray injection, an ignition event, or a flame propagation can be visualized. Time scales of such phenomena can be estimated from the time-resolved data. An example in which cycle-resolved imaging can provide unique information is in homogeneous-charge compression-ignition (HCCI) engines,[3,4] in which the appearance and growth of autoignition kernels can be studied.[5] Another application is in direct-injection stratified-charge (DISC) engines,[6,7] in which it is essential that the stratified fuel charge is transported to the vicinity of the spark plug and that it arrives there at the time of ignition. The whole transport process from the injector to the spark plug in individual cycles can be studied and analyzed with high-speed imaging. This means that any instabilities in the fuel-injection process can be studied.

High-speed photography of flame emission has been used for cycle-resolved studies of flame propagation, providing line-of-sight information of flame propagation.[8] To study fuel sprays, researchers used high-speed photography in combination with laser illumination, with high-repetition-rate Cu^+ lasers.[9,10] Cycle-resolved point and 2-D flow measurements by use of laser Doppler velocimetry[11] and particle image velocimetry[12,13] have been reported. Planar laser-induced fluorescence (PLIF) imaging has been used to acquire image pairs in engines by use of double-pulsed lasers for fuel tracer PLIF[10] and residual gas PLIF.[14]

As turbulent combustion taking place inside the combustion chamber is an intrinsically three-dimensional (3-D) phenomenon, 3-D measurements of relevant quantities are highly desirable. For example, 3-D data can be used to study flame or fuel-spray topology or to calculate all components of gradients.

Previous 3-D imaging in engines was achieved by researchers recording a large number of 2-D images at a fixed crank-angle degree (CAD) in different cycles and repeating this for different positions in the cylinder, thus producing mean quantities.[15] Two-dimensional imaging techniques can be extended to obtain quasi-3-D information when a stack of closely spaced planar images is rapidly recorded. This is feasible by the sweeping of the laser beam through the combustion chamber by use of a rapidly rotating mirror. The generated signals must then be imaged at a rate higher than the characteristic time scales of the in-cylinder flow and flame propagation. Instantaneous 3-D concentration measurements based on this principle have been demonstrated in jet flames by use of various laser techniques, for example, Mie scattering[16,17]; Rayleigh scattering[18]; laser-induced fluorescence (LIF) from O_2,[19] OH,[20] acetone,[17] and biacetyl[18,19]; and laser-induced incandescence.[21] In engines a slightly different approach, in which a laser beam consisting of four discrete wavelengths is formed into four sheets by use of a dispersive prism, has been used for instantaneous 3-D imaging.[22] Obviously, this approach can be used only for Mie scattering, and not fluorescence, as four completely different laser wavelengths are involved.

In this paper we present a laser and detector system for cycle-resolved engine studies by use of high-repetition-rate PLIF imaging. The system can be used for acquiring a sequence of as many as eight images with repetition rates ranging from 100 Hz to as high as 100 MHz. The laser source is a custom-designed Nd:YAG laser cluster consisting of four individual pulsed high-power Nd:YAG lasers that are combined into one unit. The detector is a modified high-speed camera based on eight intensified CCD cameras. By exposing the eight cameras in series, one can capture fast image sequences. The system has previously been used for high-repetition-rate laser diagnostics of nonpremixed jet flames[23] and expanding premixed flame kernels.[24]

In this paper, true single-cycle-resolved OH radical concentrations and fuel tracer concentrations, measured in three types of IC engines, are presented. The recorded sequences comprise eight PLIF images, with a spacing ranging from fractions of a CAD to several CADs. The engines studied are a small SI engine for small-scale electricity production, an automotive DISC engine, and a prototype HCCI engine. Turbulent flame propagation, stratified-charge injection and ignition, and HCCI autoignition are captured in real time, providing unique insight into these phenomena. A first demonstration, to our knowledge, of 3-D PLIF imaging in engines, of fuel concentrations in the HCCI engine, is also presented.

2. Experimental Techniques

A. Nd:YAG Laser Cluster

The laser cluster consists of four standard flash-lamp-pumped Nd:YAG lasers (BMI/CSF-Thomson, France). The laser cluster is illustrated in Fig. 1. Each laser consists of a Q-switched oscillator and a single amplifier. When the Q switch is switched twice during the flash-lamp pumping, each of the Nd:YAG lasers is fired twice with a short time separation.

The beams from the four lasers are combined by use of the scheme illustrated in Fig. 1. The laser beam from the first laser is converted from 1064 into 532 nm, with a second-harmonic-generation crystal. This beam is then combined with the 1064-nm beam from the second laser by use of a dichroic mirror, reflecting 532 nm and transmitting 1064 nm. The combined beams then pass through the second-harmonic-generation crystal of the second laser: The 532-nm beam passes unaffected while the 1064-nm beam is converted into 532 nm. The same combining procedure is then repeated two more times until all beams are overlapped. The many optical components in the beam path of the first lasers introduce energy losses and beam profile degradation; however, the energy losses can be compensated for by

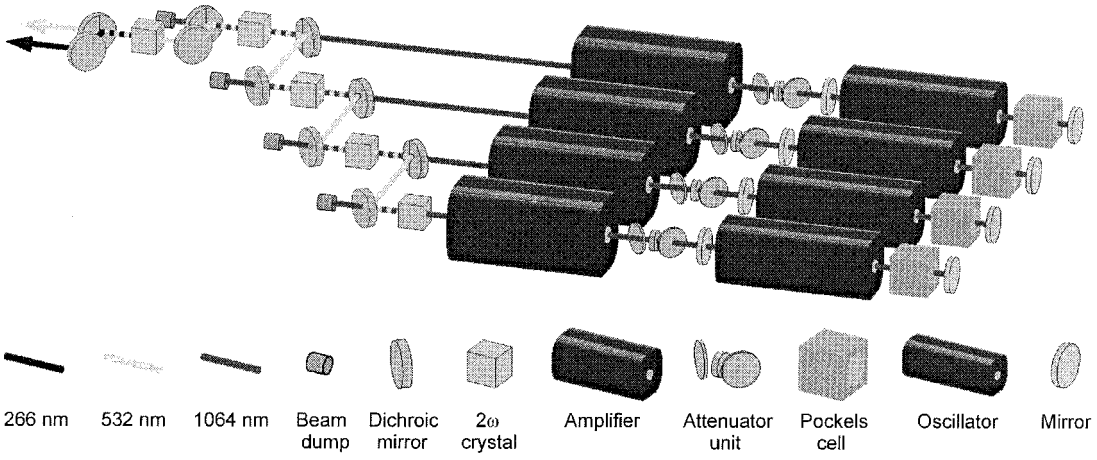

Fig. 1. Schematic overview of the Nd:YAG laser cluster, consisting of four individual laser units and beam-combining optics.

an increase in the flash-lamp-pumping intensity of these lasers. There is also an alternative beam-combining scheme in which a combination of beams of different polarizations is used. The advantage of this scheme is fewer optical components, which minimizes energy losses; however, the alignment is more critical. After the beam-combining optics, there is an option to insert a fourth-harmonic-generation crystal, for generation of 266-nm radiation.

The four individual lasers can be fired in series with a time delay of as much as 100 ms, corresponding to the overall repetition frequency of 10 Hz. The time separation between two double pulses from one of the lasers can be adjusted from 25 to 145 μs. It is limited by the length of the flash-lamp-pumping pulse and the gain build-up time in the cavity. By interleaving the double pulses from the four lasers, one can reduce the time separation between pulses to 6.25 μs (= 25 μs/4) when equal time separations are desired. The laser pulses do not have to be equally spaced, however, because each laser timing is individually controllable. Maximum pulse energies of the lasers are given in Table 1. The pulse energy in double-pulse operation depends on the pulse separation time, with a maximum around 80 μs.

B. Dye Laser

To convert the 532-nm output from the Nd:YAG laser cluster to other wavelengths, we use a dye laser pumped by the Nd:YAG laser cluster. The dye laser (ND60, Continum) is narrow band (0.08 cm^{-1}) and wavelength tunable, with a harmonic-generation unit attached to it.

For excitation of the OH radical, laser light with a wavelength of 283 nm was used. This wavelength is generated by use of a Rhodamine 590 dye solution in methanol, with subsequent frequency doubling of the dye laser output by use of a KDP crystal.

When the dye laser is pumped by a rapid sequence of pulses from the multiple Nd:YAG laser, its performance deteriorates. The output energy and the beam profile are deteriorated for consecutive pulses in a sequence. This is due to the limited time available for the dye solution in the dye cells to be exchanged between consecutive pumping pulses. The output energies of a three-pulse sequence from the dye laser oscillator are shown in Fig. 2 as a function of pulse separation. The time it takes to exchange the dye solution in the pumped volume is around 700 μs. This matches well with the trend in Fig. 2, in which the energy of pulses 2 and 3 decreases rapidly in the region of 400–900 μs. The dye laser perfor-

Table 1. Nd:YAG Laser Cluster Pulse Energies

Operation[a]	Pulse Energy (mJ)
532 nm, SPO	500
532 nm, DPO (80 μs)	200
266 nm, SPO	90
266 nm, DPO (80 μs)	45

[a]SPO, single-pulse operation. DPO, double-pulse operation.

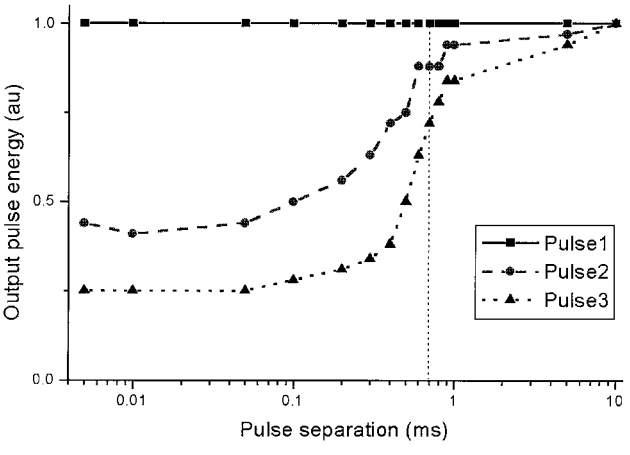

Fig. 2. Output energies from the dye laser oscillator when pumped by a burst of three pulses from the Nd:YAG cluster, with varying time separation. The dotted curve corresponds to the dye-solution exchange time.

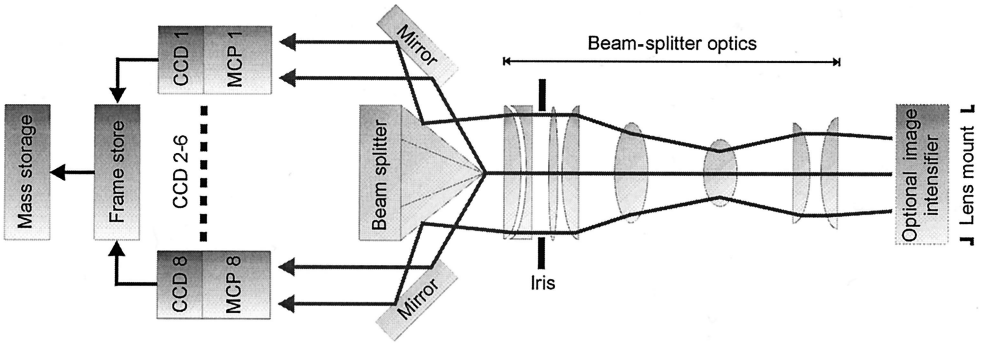

Fig. 3. Schematic overview of the high-speed camera, consisting of eight individual CCD units.

mance at high repetition rates is expected to improve if the dye circulation speed is increased.

The observed energy decay can be compensated for by reduction of the pumping energy in the first pulses until all pulses out from the dye laser have the same energy. Unfortunately, this procedure strongly reduces the output energy in each pulse compared with the output energy from single-pulse pumping. The beam profiles also gradually deteriorate when the pulse separation is decreased. These problems can be compensated for by spatial beam filtering, at the cost of decreased intensity, and by beam profile monitoring and correction. The latter has been demonstrated in a combustion cell experiment[25]; a similar scheme is also used in Ref. 26.

C. Detector

The detector is a custom-modified high-speed framing camera (Imacon 468, DRS Hadland, UK). Extra triggering features and an optional image intensifier at its input have been added. The high framing speed is achieved by exposure of eight individual CCDs sequentially, by use of short exposure times. A schematic overview of the camera is shown in Fig. 3. The high-speed camera employs a single optical input with subsequent split up to the individual CCD detectors. This approach has the advantage of imaging the same object with all cameras and minimizing distortions. An eight-facet pyramid beam splitter is used to divide the incoming light into eight separate optical paths. Mirrors then relay this light to the CCD units. A motorized iris positioned within the beam-splitter optics is used to control the system aperture and depth of field. The individual CCD modules consist of an image intensifier of the microchannel plate (MCP) type and a CCD image sensor. The MCP is fiber optically coupled to the CCD to ensure maximum coupling efficiency. Each CCD has 576×385 pixels, with a pixel size of $22\ \mu m \times 22\ \mu m$. The signals from the CCDs are digitized to 8 bits, stored in digital frame stores within the camera, and transferred to the controlling computer via a fiber-optic link.

The optional image intensifier is attached at the front of the optical system, positioned in the image plane of the camera. It increases the sensitivity of the camera by as much as two orders of magnitude. It also makes it UV sensitive by converting the incoming UV light into visible light, which is transmitted and detected by the original optical system. It is a three-stage image intensifier, in which submicrosecond decay phosphors have been used to make imaging of fast events possible. The use of the extra image intensifier reduces the spatial resolution of the detector system by approximately a factor of 2.5.

Exposure times, gains, and trigger delays are individually programmable for each CCD. Each CCD unit can be exposed as many as four times within each image sequence. The minimum time between consecutive images is 10 ns; when the extra intensifier is used, this minimum time separation increases to 1 μs. The minimal time interval between two consecutive eight-image sequences is governed by the transfer rate to the mass storage device and is currently limited to a few seconds. The possibility of using different gains for different CCDs allows events to be captured when the signal intensity varies strongly in time, as the dynamic range between images is increased.

D. Synchronization

The laser system can be triggered in several ways, providing flexibility for different applications. It can be triggered at 10 Hz internally or from an external source. The individual lasers are then fired with individually adjustable preset delays from the master trigger. This approach can be used when an engine is operated at 1200 rpm (corresponding to 10 Hz), and a single trigger pulse from each engine cycle is used.

A more general alternative, in which an arm-and-fire sequence is used to trigger the laser to a single external event, is applicable to all engine speeds and is illustrated in Fig. 4. The laser is continuously operated at 10 Hz to ensure a constant heat dissipation and thus thermal stability of the laser crystals. When the rising edge of an external trigger pulse is detected, the 10-Hz laser operation is temporarily interrupted, and the laser is put into a waiting mode. At the falling edge of the trigger pulse (which is set to correspond to a certain crank angle in the engine cycle) a laser-pulse burst is fired with the individually

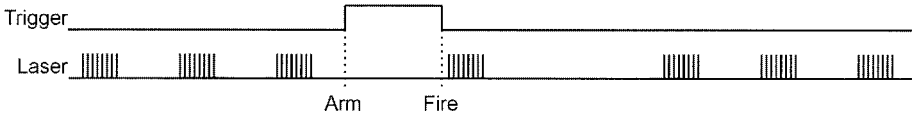

Fig. 4. Timing diagram of the arm-and-fire trigger option.

adjustable preset delays for each laser. After this externally triggered pulse train is fired, the laser returns to the original 10-Hz repetition rate.

The laser sends out trigger signals to the detector 500 ns before the opening of each Q switch. The eight CCDs in the high-speed camera are then triggered by these individual trigger signals from each laser. It is also possible to trigger the CCDs by use of only one common master trigger, which starts an exposure series with preset delays.

E. Cycle-Resolved Imaging

Two LIF techniques have been used to extract cycle-resolved information from the engines. Fuel tracer PLIF has been used to measure fuel concentrations, and OH PLIF has been used to measure OH radical concentrations, which is a good marker for the flame-front position.

In fuel tracer PLIF, a fluorescing tracer species, with physical properties resembling the fuel, is added to a nonfluorescing fuel. With a proper choice of tracer, the tracer concentration is proportional to the overall fuel concentration. In the SI and DISC engines, 3-pentanone (6% and 10%, respectively) was used as tracer species for the iso-octane fuel, and in the HCCI engine, acetone (10%) was used as tracer species for the ethanol fuel. For a more detailed discussion of fuel tracers and fuel tracer PLIF, see Ref. 27. The recorded fuel tracer LIF images represent pure fluorescence intensity and not quantitative fuel concentrations, as no quenching corrections were performed. However, the qualitative fuel-concentration information is sufficient for studying the temporal development of, e.g., flame fronts or fuel decomposition.

The OH radical is formed close to the flame front, and it is often used as a flame-front marker. It is formed by fast two-body reactions and is consumed by slower three-body recombination reactions.[28] In a premixed flame the OH produced at the flame front is slowly consumed in the burnt gases and thus acts as a marker of both the flame front and, partially, the burnt gases. An example in which OH PLIF was used for studies of flame-front structures in SI engines can be found in Ref. 29.

For fuel tracer PLIF the frequency-quadrupled output from the Nd:YAG laser cluster, $\lambda = 266$ nm, was used to excite the 3-pentanone or acetone tracer molecules. At 266 nm the energy per pulse was around 30 mJ for an eight-pulse sequence. For OH PLIF the frequency-doubled output from the Nd:YAG laser cluster, $\lambda = 532$ nm, was used to pump a dye laser. The dye laser radiation around 566 nm was then frequency doubled to around 283 nm, exciting the $Q_1(8)$ transition in the $v'' = 0, v' = 1$ band of the $A^2\Sigma^+ \leftarrow X^2\Pi$ system of OH. At 283 nm the energy per pulse was 5–12 mJ for a four-pulse sequence.

The laser beam was focused into a sheet, which was typically 20–50-mm wide and 200–400-μm thick, by a combination of cylindrical and spherical lenses. The LIF signal is generated where this light sheet intersects the fuel or flame and is detected at right angles by the high-speed camera. When the fluorescence is detected through a window in the piston, a fixed mirror (UV enhanced) inside the piston extension is used to reflect the signal to the camera. Depending on the wavelength of the fluorescence and the optical access in the specific engine, either an achromatic UV transparent quartz lens ($f = 100$ mm, $f\# = 2$) or a glass lens ($f = 50$ mm, $f\# = 1.2$) was attached to the camera to collect the signal.

For the fuel tracer PLIF, two filters were used in front of the camera. The first was a long-pass filter transmitting the LIF signal, which has a maximum around 430 nm, and rejecting scattered laser light at 266 nm. The second was a short-pass filter transmitting the LIF signal and rejecting fluorescence from oil residues on the cylinder surfaces and windows. For the OH PLIF, two filters were used in front of the camera: a long-pass filter, transmitting the LIF signal around 310 nm and rejecting scattered laser light at 283 nm, and a bandpass filter, transmitting the LIF signal and rejecting scattered residual dye laser light at 566 nm.

F. Three-Dimensional Laser-Induced Fluorescence Imaging

Three-dimensional fuel visualization is feasible by the sweeping of the laser beam through the combustion chamber by use of a rapidly rotating mirror. With this technique, stacks of eight closely spaced planar images have been recorded in the HCCI engine. The experimental setup is illustrated in Fig. 5. The Nd:YAG laser cluster fired sequences of eight laser pulses, with a time separation of 10 μs between the pulses. The output was frequency quadrupled to give 266-nm radiation, with an energy around 30 mJ/pulse. A galvanometric scanning mirror (GSI Lumonics) was used to reflect the colinear beams at right angles into the combustion chamber, through the quartz cylinder liner. A cylindrical lens ($f = -100$ mm) and a spherical lens ($f = +1000$ mm) were used to form light sheets of a 50 mm $\times$ 0.25 mm cross section. By the positioning of the scanning mirror at the focal point of the spherical lens, the light sheets became parallel. The scanning mirror was operated at 100 Hz, which corresponded to a laser-sheet displacement speed of 50 m/s inside the combustion

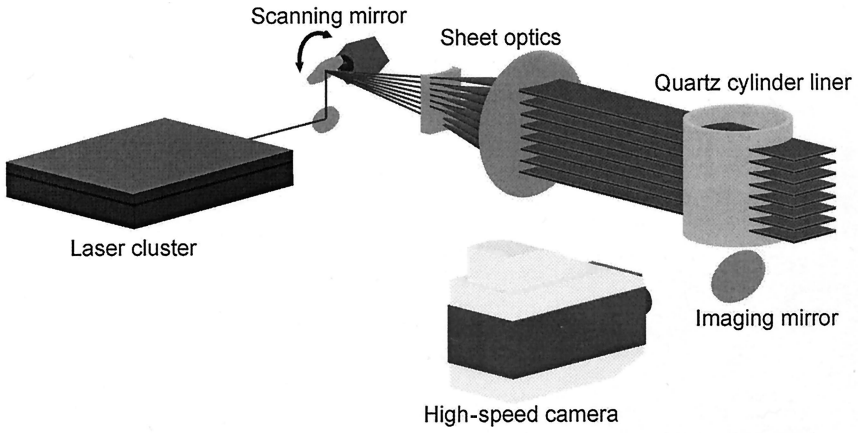

Fig. 5. Three-dimensional LIF imaging setup.

chamber. The delay of 10 μs between pulses resulted in a separation of 0.5 mm between the laser sheets. The total acquisition time of the 3-D data, 70 μs (corresponding to 0.5 CAD), was sufficiently short to freeze the fuel distribution in the engine, which was checked when the image series was recorded without use of the scanning mirror.

The high-speed camera, equipped with the achromatic quartz lens, was used to detect the fluorescence signal from the eight measurement planes, through the window in the piston. The same filters as described for the high-repetition-rate fuel tracer PLIF in Sub-section 2.E were used. The imaged region corresponded to 88 mm × 43 mm × 3.5 mm, and the depth of field of the imaging optics exceeded the dimensions of the measurement volume.

The movement of the scanning mirror was controlled by a signal generator and synchronized to the engine operation. The signal generator produced ten sinus pulses with a period of 10 ms and was trigged by a pulse from the engine control system, corresponding to a specific crank-angle position in each combustion cycle. The operation of the engine at 1200 rpm, corresponding to 10 Hz, resulted in a mirror movement of 100 Hz. The Nd:YAG laser cluster was triggered by the same pulse from the engine control system and thus also became synchronized to the mirror. By adjustment of the delay from this pulse to the start of the laser-pulse burst, the position of the laser-sheet stack inside the combustion chamber could be adjusted. The current mirror control system is thus limited to engine operation at multiples of 10 Hz.

3. Measurement Objects

A. Spark-Ignition Engine

For the initial development of the cycle-resolved imaging technique, we used a small SI engine. It is a commercially available, single-cylinder, four-stroke, side-valve, SI engine (Briggs & Stratton). A water-cooled cylinder head with three quartz windows replaced the original air-cooled head, leaving the original valve and port geometry unaltered. The spark plug was moved from the center of the cylinder bore to a position between the intake and the exhaust valves. This places the spark gap, and hence the early flame kernel, within the field of view; see Fig. 6, in which the optical access is shown. During the experiments the engine was run at a medium load of 2 kW, at 1200 rpm, with iso-octane as fuel.

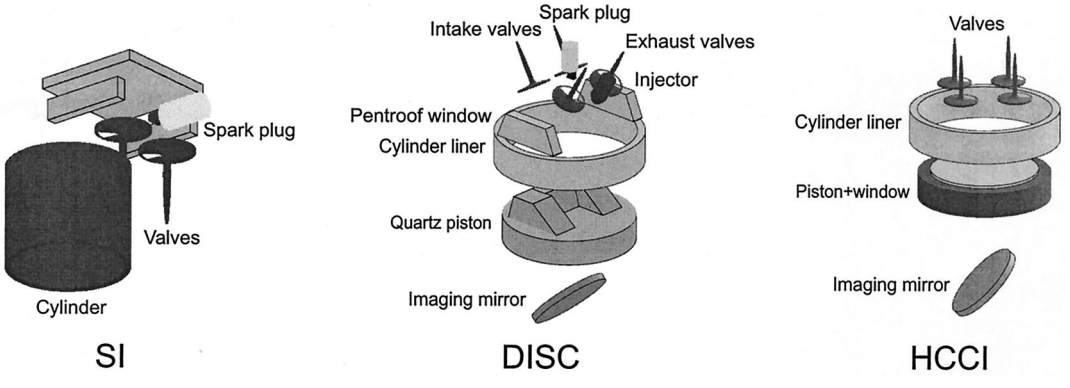

Fig. 6. Schematic overview of the optical access of the three IC engines studied: a 0.2 l/cylinder Briggs & Stratton SI engine, a 0.5 l/cylinder Volvo DISC engine, and a 1.95 l/cylinder Scania HCCI engine.

B. Direct-Injection Stratified-Charge Engine

DISC engines are in most cases SI engines in which the fuel is injected directly into the combustion chamber.[6,7] With this technique it is possible to achieve a stratified charge. The advantage of this is that the engine can be operated at lean conditions. This implies that less throttling is necessary at low loads. Other advantages with DISC are related to the cooling effect of the fuel spray, which together with a more dense charge, will increase both power rating and fuel efficiency. The design goal for the combustion system is to achieve a slightly rich mixture in the vicinity of the spark plug at the time of ignition while the charge, as a total, shall remain lean.

The investigated engine was of the swirl type and featured a spray-guiding bowl-in-piston design. The engine was a modified single-cylinder Volvo DISC equipped with pentroof windows and a transparent cylinder liner that provided optical access from the sides; see Fig. 6. Two piston crowns with different geometry were tested. One had a production-type geometry with a quartz window in the piston bowl, allowing optical access from below (Bowditch design). The other one had a simplified geometry for basic understanding and validation of computational fluid dynamics modeling. This piston was machined from a single piece of quartz to maximize the optical access. For the experiments reported here, iso-octane was used as fuel ($\lambda = 2.3$). The engine was run at 2000 rpm, in a 5:1 skip-fire mode.

C. Homogeneous-Charge Compression-Ignition Engine

In the type of HCCI engine studied, a homogeneous mixture is formed in the intake manifold.[4] The mixture is then drawn into the cylinder, during the intake stroke. At the end of the compression stroke, the temperature and pressure of the mixture exceeds the ignition point of the fuel. Auto-ignition occurs at many points almost simultaneously, where local conditions are most favorable. The whole mixture is then consumed very rapidly, in approximately 1–2 ms. To avoid too fast combustion, one must use lean or diluted mixtures. The benefits with the HCCI engine are low emissions of nitrogen oxides and soot and high efficiency. The drawback compared with the spark-ignited engine and the Diesel engine is that a more complex control system is required to achieve ignition at a desired crank-angle position.

The engine used for the HCCI studies was a Scania D12 single-cylinder engine, equipped with Bowditch-type optical access.[5] A large window in the piston and the quartz cylinder liner allowed optical access to the major part of the combustion chamber; see Fig. 6. Ethanol or iso-octane was used as fuel, and for these fuels the compression ratio was set to 16:1. A lean fuel–air mixture, $\lambda = 4.0$, was used. For the experiments presented here, the engine was operated at 1200 rpm.

4. Data Postprocessing

Owing to nonperfect alignment of the individual CCD modules with respect to the optical axis, the imaged regions do not overlap perfectly. There are small shifts and rotations between the images recorded with the eight CCD cameras. The displacements between the CCDs can be corrected by a geometrical transform (warping), which maps the images from the different CCDs to a common reference image coordinate system. The geometric transform is a vector function that maps each pixel to a new position.[30]

A background image recorded with the fuel injection switched off has been subtracted from most images. The image pixels have been binned together 2×2. This reduces noise without decreasing the resolution, which is limited to around 2.5 pixels by the extra image intensifier.

The fuel tracer PLIF images acquired in the SI and HCCI engines have been compensated for inhomogeneities in the laser intensity profiles. Unburned regions were identified in mean fuel tracer PLIF images, averaged over 25 cycles. From the unburned regions the laser profile was extracted, and individual images were then divided by this profile.[31] In the HCCI engine the laser light is gradually attenuated by absorption, as the sheet passes through the cylinder. To compensate for this, the mean absorption curve was extracted from the mean fuel tracer PLIF images, and absorption in individual images was compensated for by use of this curve.

For visualization of the 3-D fuel tracer PLIF data, we used a shape-based interpolation scheme. The eight 2-D images are first thresholded to produce eight isoconcentration curves. Shape-based interpolation is then used to create new isoconcentration curves, filling the gaps between the eight original image planes. In the data presented in this paper, seven curves were created between each original curve. Finally, a 3-D isoconcentration surface is calculated from these isoconcentration curves. The process is described in detail in Ref. 32.

5. Results and Discussion

A. Spark-Ignition Engine

In the Briggs & Stratton SI engine, early flame propagation has been captured by rapidly sequenced fuel tracer and OH PLIF. An example of fuel tracer PLIF is shown in Fig. 7, where eight consecutive images recorded in the same combustion cycle are presented. The combustion chamber is viewed from above with the spark plug located to the upper right; see the photo to the left in Fig. 7. The intensity in the PLIF images is proportional to fuel concentration, which means that bright regions correspond to unburned gases and dark regions correspond to burnt gases. The turbulent flame propagation is illustrated by the expansion of the burnt regions through the sequence. The time separation between consecutive images is 100 μs, which corresponds to 0.72 CAD. The first image is acquired at 5 CAD after top dead center (ATDC), which is 15 CAD after the time of ignition. The appearance of isolated flame islands in the sequence is an effect of 3-D flame wrinkling in and out of the 2-D laser sheet.

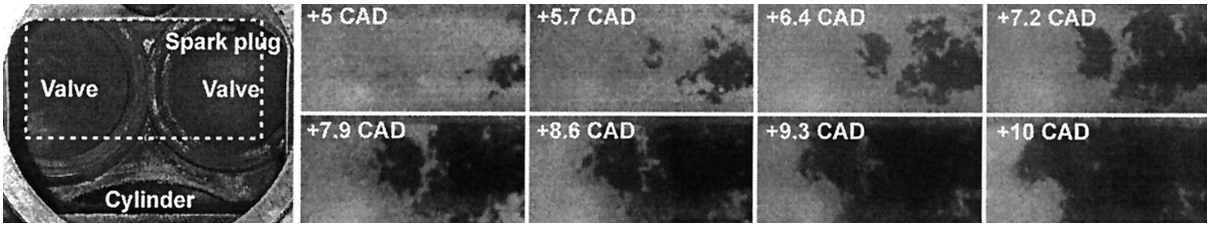

Fig. 7. Cycle-resolved fuel tracer PLIF sequence recorded in a SI engine. The time separation between consecutive images corresponds to 100 μs (0.72 CAD); time of ignition: −10 CAD. The imaged region was 50 mm × 25 mm, and is shown to the left.

One example of a parameter that can be calculated only from this type of time-resolved flame data is the local flame-front propagation velocity. Two sequential images were then first segmented into burned and unburned regions. In the resulting binary images, smooth flame-front curves were identified. A number of corresponding points, e.g., points of high curvature, were identified in the two flame-front curves. For these corresponding points the flame-front displacement velocity was calculated directly. For intermediate points on the curves, corresponding points were located by use of interpolation along the curves.

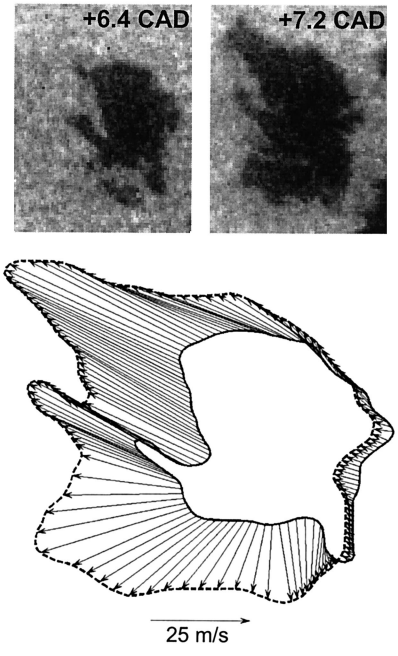

Fig. 8. Local flame-front propagation velocity, evaluated from flame-front contours extracted from the images shown at the top. The calculation is performed on the data corresponding to the two images in the upper right of Fig. 7.

In Fig. 8 an example is shown, in which the flame-front velocity is calculated from the sequence in Fig. 7. The flame-front contours at +6.4 and +7.2 CAD are shown; the lengths of the arrows connecting the two contours are proportional to the local propagation velocity at the front. Apart from the expansion of the flame kernel, there is also a convection, mainly to the left in the image. The mean velocity along the flame contour was found to be 26 m/s, with a maximum of 54 m/s. It should be noted, however, that the measured velocity is not the turbulent flame propagation velocity, as it is a superposition of convection and propagation. To determine the actual turbulent flame velocity, one must measure the gas velocity field simultaneously.[33]

In Fig. 9 an example of an OH PLIF sequence is shown. Regions appearing bright in the PLIF images indicate the presence of OH radicals, which are formed at the flame front and survive in the burnt gases. In the images the position of the flame front can be identified as the edge of the bright OH regions. To enhance the gradient at this edge, we used a nonlinear diffusion-filtering algorithm described in Ref. 34. The time spacing between the four images in this series is 100 μs, and the first image starts at 9 CAD ATDC. In the first image of the series a small flame is seen in the vicinity of the spark plug; with increasing time the flame kernel then expands into fresh mixture. The OH data appear as an inverse of the fuel-concentration data, and both can be used to identify the propagating flame front.

B. Direct-Injection Stratified-Charge Engine

In a DISC engine an overall lean operation is made possible by use of a stratified fuel charge, which provides a rich and ignitable fuel mixture at the location of the spark. For stable engine operation, it is vital

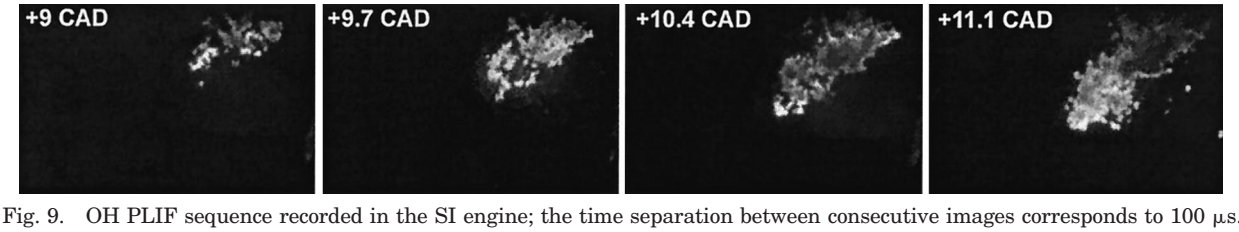

Fig. 9. OH PLIF sequence recorded in the SI engine; the time separation between consecutive images corresponds to 100 μs.

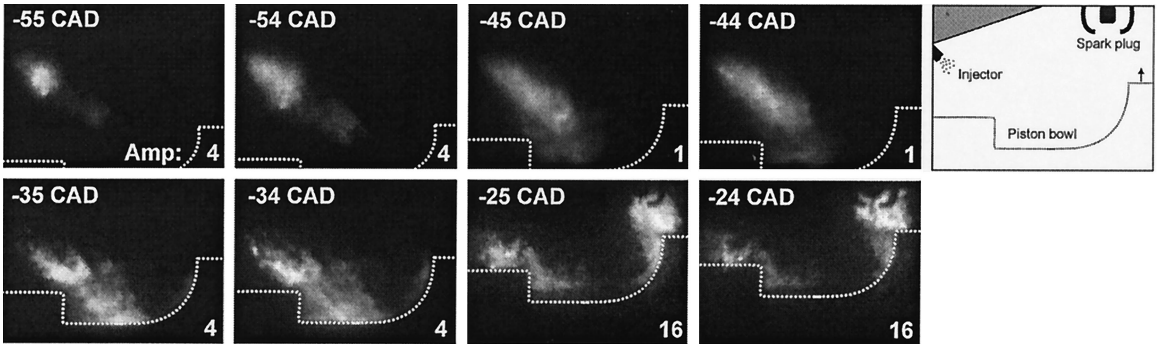

Fig. 10. Fuel tracer PLIF sequence of fuel injection in the DISC engine; time of ignition: −23 CAD. The fuel distribution in a plane 1 mm behind the spark plug is viewed through a side window. The imaged region corresponds to 61 mm × 45 mm and is shown to the right; the piston position is indicated by a dashed line in each image. The relative gain amplification factors of the individual cameras are indicated to the lower right in the images.

that the rich fuel charge arrives at the spark plug at the time of ignition.

In Fig. 10 the fuel injection is captured in a fuel tracer PLIF sequence, covering 31 CAD. The fuel injection is viewed from the side, through the cylinder liner and pentroof window. The fluorescence signal from inside the piston bowl also passes through the sidewalls of the quartz piston. At 55 CAD before top dead center (BTDC) the first part of the fuel charge is seen leaving the injector. At 45 CAD BTDC the tip of the fuel spray is approaching the bottom of the piston bowl. The shape of the piston crown in combination with spray momentum and swirl–tumble motion then guides the fuel upward. In the last images, at 25–24 CAD BTDC, the fuel has left the piston bowl, traveling upward in the direction of the spark plug. In the upper part of the image, one can see that the fuel charge has arrived at the spark plug, which is seen as a dark shadow. The spark discharge begins at 23 CAD BTDC and has a duration of approximately 10 CAD, so the fuel seems to have arrived at the spark plug at the correct time. As the fuel concentration shows a large variation during the different phases of the injection, different gains have been used for the individual CCDs in the high-speed camera. For example, the amplification in image 8 is 16 times larger than in image 3. This results in a larger dynamic range than 8 bits for the sequence as a whole, but the different gain settings must be taken into consideration if the fluorescence signals in the different images are to be compared quantitatively.

Fuel transport and initial flame propagation in four cycles are shown in Fig. 11. The fuel tracer PLIF in a horizontal plane, 1 mm below the spark gap, was detected through the window in the piston bowl. In the first images of the sequences, the fuel distributions at the location of the spark plug, which is indicated at the top of Fig. 12, are seen. The bright regions correspond to the fuel cloud, which moves in the direction from the spark plug into fresh gas, which appears dark. From the sequences it is evident that the size of the fuel-rich region at the spark plug location varies from cycle to cycle. At the bottom of the images, at the location of the spark plug, the start of flame propagation can be seen in the imaged plane (start of ignition: 27 CAD BTDC). The location of the flame is indicated by the appearance of dark regions that are due to consumption of fuel. In sequences a and b the propagation of the flame in the fuel-rich region can be followed. Cycle-

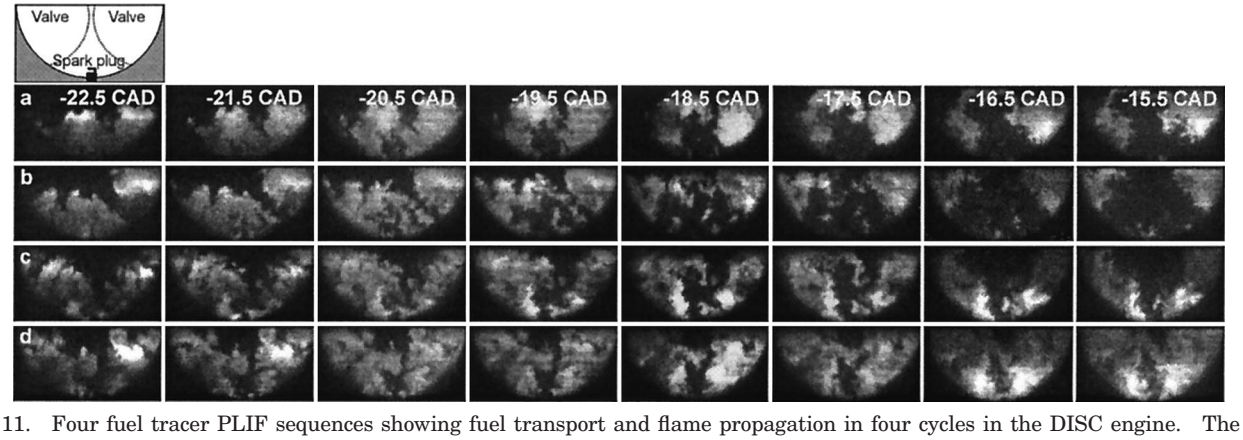

Fig. 11. Four fuel tracer PLIF sequences showing fuel transport and flame propagation in four cycles in the DISC engine. The fuel distribution in a plane 1 mm below the spark plug is viewed through the piston; the imaged region was 26 mm × 13 mm and is shown above the sequences.

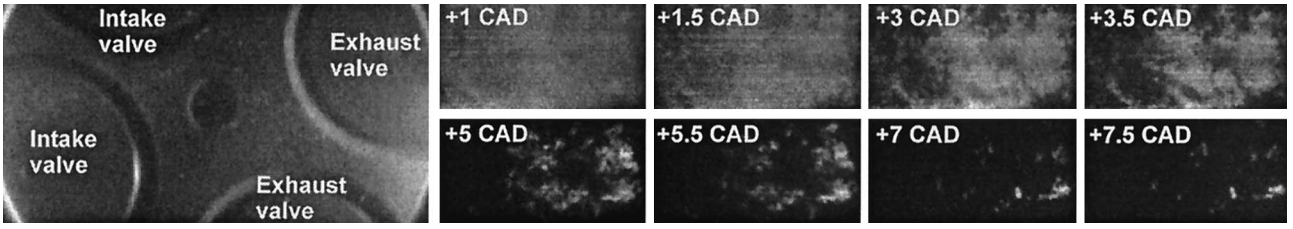

Fig. 12. Fuel tracer PLIF sequence recorded in the HCCI engine. The fuel distribution in a plane in the center of the combustion chamber was imaged through the piston. The imaged region corresponds to 95 mm × 50 mm and is shown to the left.

to-cycle variations in fuel transport lead to variations in flame propagation speed; for example, the flame in sequence b has expanded more than the flame in sequence a at the end of the sequence. In sequences c and d the rich fuel charge is spread more to the sides and not in the center in the first frame. In these two sequences it is more difficult to identify burned regions, and in sequence d the major part of the viewed regions is filled with unburned fuel at the end of the sequence. Figure 11 illustrates the use of high-repetition-rate imaging to study cycle-to-cycle variations of complex events, in this case, stratified-charge transport, and the following ignition and flame propagation. In the present example, a strong correlation was found between the amount of fuel present around the spark plug and the amount of fuel burned at the end of the sequence.

C. Homogeneous-Charge Compression-Ignition Engine

In a HCCI engine the premixed fuel–air mixture autoignites by compression. In Fig. 12 a sequence covering the major part of a combustion event in the HCCI engine is shown, covering 6.5 CAD. The fuel distribution is viewed from below through the piston window. The field of view is shown to the left in Fig. 12. In the first image (1 CAD ATDC) a homogeneous fuel distribution is seen. In the next image several small dark regions can be found to the left, to the right, and in the upper part of the image, indicating that the reactions that consume fuel have started. These chemical reactions are initiated by the temperature rise associated with the compression of the gas. The fuel in these regions is then consumed further in the next images; the regions spread, and new regions of fuel consumption also appear. The HCCI combustion is rapid; in 3.5 CAD most of the fuel is consumed, and in the end (7.5 CAD ATDC) only small separated islands of fuel remain. The use of unequal time spacing between images throughout the series allows a long event to be captured, while short-term changes are still captured between image pairs.

Just by studying one time-resolved HCCI cycle, we can make several observations regarding the HCCI combustion process. Figure 12 indicates that there is no propagating flame in the HCCI engine, as in a SI engine. Regions of fuel consumption gradually grow darker and darker rather than propagating. This indicates that reactions are taking place everywhere simultaneously but at different rates as local inhomogeneties in temperature or fuel concentration favor reactions in certain regions. However, later in the combustion phase, sharp fuel-concentration gradients can be found in some regions, and the fuel distribution in these regions is similar in appearance to the fuel distribution associated with propagating flames in, e.g., SI engines. A possible explanation for the observed fuel distribution fields is that the combustion starts with a comparatively slow local fuel oxidation, and then a transition into a faster reaction regime takes place at some locations in the combustion chamber, while gradual oxidation is still ongoing in other locations. Compression of unburned regions by the expanding hot product gases also leads to a sharpening of structures. It should also be noted that new ignition kernels develop during the entire combustion event. By comparing a large number of cycles, in a fashion similar to Fig. 11, we found that reactions start in different regions of the combustion chamber in different cycles. The starting time of reactions and the number of regions in which reactions take place also varies between cycles.

It is possible to simultaneously record LIF and flame emission by use of the high-repetition-rate diagnostic system; in Fig. 13 an example is shown. Directly after each of the four fuel tracer PLIF exposures, a 15-μs exposure of the flame emission is recorded. As the exposure time is much shorter than the time between PLIF exposures (138 μs), the emission images can be considered simultaneous with the PLIF images. In the HCCI engine the flame emission mainly consists of chemiluminescence light, as only low levels of soot are produced during combustion. The bright regions in the emission images thus correspond to burning gases. Even though flame-emission imaging provides only line-of-sight information on flame location, the flat geometry of the combustion chamber (diameter = 127 mm, height = 10 mm) at top dead center allows an approximate localization of flame position. Thus, as expected, the bright regions of unconsumed fuel in the PLIF images correspond to dark unburned regions in the flame-emission images. The simultaneous imaging of LIF and emission is a good test of the fuel tracer technique in the HCCI environment. The good match between flame and fuel structures in the present case indicates that the fuel tracer PLIF technique works satisfactory in the HCCI engine.

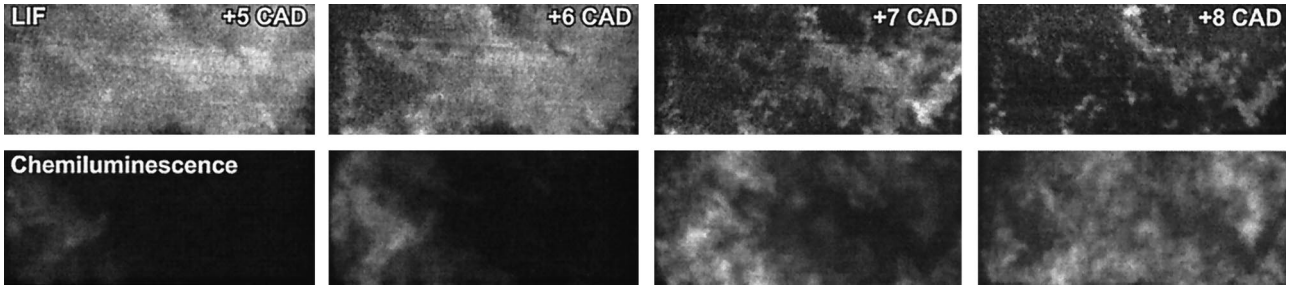

Fig. 13. Simultaneously recorded fuel tracer PLIF (upper row) and chemiluminescence light (bottom row) in the HCCI engine.

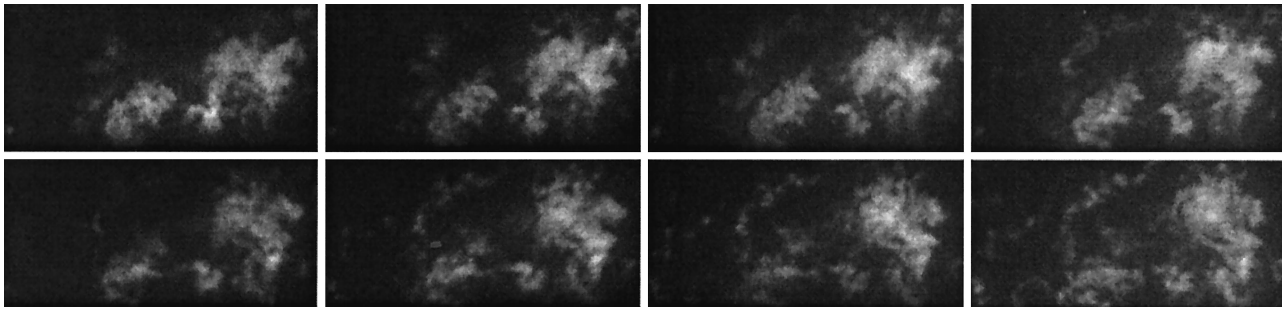

Fig. 14. Three-dimensional fuel tracer LIF, eight equidistant and parallel 2-D cuts of the fuel distribution in the HCCI engine cylinder are shown. The image separation corresponds to 0.5 mm. The 3-D data were recorded at 6 CAD ATDC.

D. Three-Dimensional Fuel Visualization

A 3-D fuel-concentration data set is shown in Fig. 14. Fuel tracer PLIF in eight equidistant planes in the cylinder was recorded at 6 CAD ATDC; the displayed data cover a volume of 88 mm $\times$ 43 mm $\times$ 3.5 mm. The images are shown from top to bottom, with the first image recorded closest to the valves. The data cover approximately 35% (3.5 mm/10 mm) of the combustion chamber height. From the data the relation between the size of structures in all three directions can be studied. In Fig. 15 a three-dimensional isoconcentration surface, calculated from the data shown in Fig. 14, is shown. It corresponds to 16% of the maximum fuel tracer LIF signal. The 3-D surface is viewed from the direction of the image in the upper left in Fig. 14; in the image the spacing between image planes has been exaggerated for a better display of the data. The 3-D representations can be used to analyze the topology of the unburned fuel structures. For example, it is possible to distinguish whether a structure that appears as an island in one of the 2-D images is a real separate island or a 3-D wrinkling effect in and out of the image plane. It is also possible to determine if the multiple autoignition kernels observed in the 2-D images are really separated or connected outside one of the image planes.

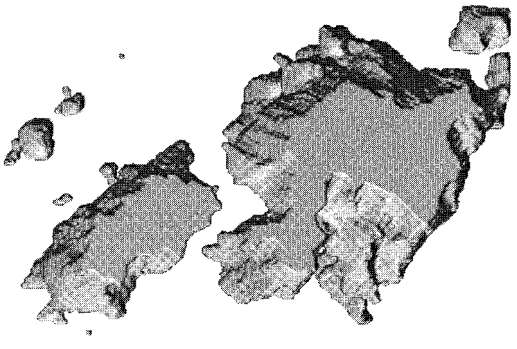

Fig. 15. Three-dimensional fuel isoconcentration surface, calculated from data shown in Fig. 14.

6. Conclusions

We have presented a unique laser diagnostic system for collecting sequences of as many as eight PLIF images within one engine cycle. This new type of single-cycle-resolved imaging data recorded by the system provides unique insight into various inherently time-dependent IC engine phenomena. Cycle-to-cycle variations of complex processes, such as stratified-charge injection and ignition, can be captured. The high repetition rate of the laser also makes 3-D measurements possible by the sweeping of the laser beams with a rapidly rotating mirror. The system can be triggered to arbitrary external events and can be operated over a large range of time scales, which allows studies of a large variety of engine-related phenomena. The performance of the laser and detector system allows a number of established laser diagnostic methods to be used, and they can be extended to time-resolved techniques.

The high performance of the system has been demonstrated by high-repetition-rate PLIF imaging of OH and fuel concentrations in three engine types. In a SI engine, cycle-resolved turbulent flame propagation was captured, and the possibility to calculate local flame propagation speeds was

demonstrated. In a DISC engine the stratified-charge injection was visualized, and the result of cycle-to-cycle variations in fuel transport on the ensuing combustion was investigated. In the HCCI engine both the spatial and the temporal characteristics of autoignition and the combustion process were studied. In this engine, 3-D fuel concentrations were also measured.

Future research will be directed toward cycle-resolved imaging of formaldehyde (CH_2O), which is an important intermediate species in IC combustion. The Nd:YAG laser cluster is potentially a good light source for one-dimensional Raman scattering, as large energies can be deposited during an adjustable time interval, avoiding high peak energies that lead to window damage or optical breakdown. Raman scattering can be used to measure absolute fuel–air ratios along a line inside the cylinder. A more general electronic control system for the scanning mirror will be designed to allow 3-D imaging at engine speeds other than 1200 rpm (10 Hz). Three-dimensional imaging of OH radicals is another goal, which can be reached only when high-repetition-rate pumping of the dye laser becomes possible. In the future, efforts will be directed at improving the performance of the dye laser and at investigating other means of wavelength generation.

The authors thank Volvo Car Corporation, Scania CV AB, the Swedish National Energy Administration, the Swedish Research Council, "Programrådet för Fordonsteknisk Forskning," and the Center for Combustion Science and Technology for financial support. The authors thank Göran Josefsson, Volvo Technological Development Corporation, for valuable assistance in the DISC engine experiments. They also want to thank Jens Richter, WeAidU AB, for supplying the algorithm used for estimation of flame propagation velocities.

References

1. A. M. Rothrock and R. F. Selden, "Factors controlling diesel engine performance," Proc. Combust. Inst. **2,** 301–312 (1937).
2. J. Wolfrum, "Lasers in combustion: from basic theory to practical devices," Proc. Combust. Inst. **27,** 1–41 (1998).
3. P. Najt and D. E. Foster, "Compression-ignited homogeneous charge combustion," SAE Technical Paper 830264 (Society of Automotive Engineers, Warrendale, Pa., 1983).
4. R. H. Thring, "Homogeneous-charge compression-ignition (HCCI) engines," SAE Technical Paper 892068 (Society of Automotive Engineers, Warrendale, Pa., 1989).
5. A. Hultqvist, M. Christensen, B. Johansson, J. Nygren, M. Richter, J. Hult, and M. Aldén, "The HCCI combustion process in a single cycle—high-speed fuel tracer LIF and chemiluminescence imaging," SAE Technical Paper 2002-01-0424 (Society of Automotive Engineers, Warrendale, Pa., 2002).
6. T. Kume, Y. Iwamoto, K. Iida, M. Murakami, K. Akishino, and H. Ando, "Combustion control technologies for direct injection SI engine," SAE Technical Paper 960600 0424 (Society of Automotive Engineers, Warrendale, Pa., 1996).
7. F. Zhao, M.-C. Lai, and D. L. Harrington, "Automotive spark-ignited direct-injection gasoline engines," Prog. Energy Combust. Sci. **25,** 437–562 (1999).
8. D. Lee, S. Goto, I. Kim, and M. Motohashi, "Spectroscopic investigation of the combustion process in an LPG lean-burn SI engine," SAE Technical Paper 1999-01-3510 0424 (Society of Automotive Engineers, Warrendale, Pa., 1999).
9. D. E. Winterbone, D. A. Yates, E. Clough, K. K. Rao, P. Gomes, and J.-H. Sun, "Combustion in high-speed direct injection diesel engines—a comprehensive study," Proc. Inst. Mech. Eng. **208,** 223–240 (1994).
10. W. Hentschel, A. Homburg, G. Ohmsede, T. Müller, and G. Grünefeld, "Investigation of spray formation of DI gasoline hollow-cone injectors inside a pressure chamber and a glass ring engine by multiple optical techniques," SAE Technical Paper 1999-01-3660 0424 (Society of Automotive Engineers, Warrendale, Pa., 1999).
11. K. Y. Kang and Je. H. Baek, "Turbulence characteristics of tumble flow in a four-valve engine," Exp. Therm. Fluid Sci. **18,** 231–243 (1998).
12. M. Reeves, D. P. Towers, B. Tavender, and C. H. Buckberry, "A high-speed all-digital technique for cycle-resolved 2-D flow measurement and flow visualisation within SI engine cylinders," Opt. Lasers Eng. **31,** 247–261 (1999).
13. M. Reeves, D. P. Towers, B. Tavender, and C. H. Buckberry, "A technique for routine, cycle-resolved 2-D flow measurement and visualisation within SI engine cylinders in an engine development environment," presented at the 10th International Symposium on Applications of Laser Techniques to Fluid Mechanics, Lisbon, Portugal, 10–13 July 2000.
14. R. Schiessl, A. Dreizler, U. Maas, A. Grant, and P. Ewart, "Double-pulse PLIF imaging of self-ignition centers in an SI Engine," SAE Technical Paper 2001-01-1925 (Society of Automotive Engineers, Warrendale, Pa., 2001).
15. M. C. Drake, D. T. French, and T. D. Fansler, "Advanced diagnostics for minimizing hydrocarbon emissions from a direct-injection gasoline engine," Proc. Combust. Inst. **26,** 2581–2587 (1996).
16. B. Yip, J. K. Lam, M. Winter, and M. B. Long, "Time resolved 3D concentration measurements in a gas jet," Science **235,** 1209–1211 (1987).
17. B. J. Patrie, J. M. Seizman, and R. K. Hanson, "Instantaneous three-dimensional flow visualization by rapid acquisition of multiple planar flow images," Opt. Eng. **33,** 975–980 (1994).
18. B. Yip, R. L. Schmitt, and M. B. Long, "Instantaneous three-dimensional concentration measurements in turbulent jets and flames," Opt. Lett. **13,** 96–98 (1988).
19. G. Kychakoff, P. H. Paul, I. V. Cruyningen, and R. K. Hanson, "Movies and 3-D images of flowfields using planar laser-induced fluorescence," Appl. Opt. **26,** 2498–2500 (1987).
20. T. Landenfeld, A. Kremer, E. P. Hassel, J. Janica, T. Schäfer, J. Kazenwadel, C. Schulz, and J. Wolfrum, "Laser-diagnostic and numerical study of strongly swirling natural gas flames," Proc. Combust. Inst. **27,** 1023–1029 (1998).
21. J. Hult, B. Axelsson, A. Omrane, R. Collin, J. Nygren, P.-E. Bengtsson, M. Aldén, and C. F. Kaminski, "Quantitative three-dimensional imaging of soot volume fraction in turbulent non-premixed flames," Exp. Fluids (to be published).
22. J. Mantzaras, P. G. Felton, and F. V. Bracco, "Three-dimensional visualization of premixed-charge engine flames: islands of reactants and products; fractal dimensions; and homogeneity," SAE Technical Paper 881635 (Society of Automotive Engineers, Warrendale, Pa., 1988).
23. C. F. Kaminski, J. Hult, and M. Aldén, "High repetition rate planar laser induced fluorescence of OH in a turbulent non-premixed flame," Appl. Phys. B **68,** 757–760 (1999).
24. C. F. Kaminski, J. Hult, M. Aldén, S. Lindenmaier, A. Dreizler, U. Maas, and M. Baum, "Complex turbulence/chemistry interactions revealed by time resolved fluorescence and direct numerical simulations," Proc. Combust. Inst. **28,** 399–405 (2000).
25. A. Dreizler, S. Lindenmaier, U. Maas, J. Hult, M. Aldén, and

C. F. Kaminski, "Characterization of a spark ignition system by planar laser-induced fluorescence of OH at high repetition rates and comparison with chemical kinetic calculations," Appl. Phys. B **70,** 287–294 (2000).
26. J. M. Seitzman, R. K. Hanson, P. A. DeBarber, and C. F. Hess, "Application of quantitative two-line OH planar laser-induced fluorescence for temporally resolved planar thermometry in reacting flows," Appl. Opt. **33,** 4000–4012 (1994).
27. H. Neij, "Development of laser-induced fluorescence for precombustion diagnostics in spark-ignition engines," Ph.D. thesis (Lund Institute of Technology, Lund, Sweden, 1998).
28. H. B. Najm, P. H. Paul, C. J. Mueller, and P. S. Wyckoff, "On the adequacy of certain experimental observables as measurements of flame burning rate," Combust. Flame **113,** 312–332 (1998).
29. H. Becker, A. Arnold, R. Suntz, P. Monkhouse, J. Wolfrum, R. Maly, and W. Pfister, "Investigation of flame structure," Appl. Phys. B **50,** 473–478 (1990).
30. M. Sonka, V. Hlavac, and R. Boyle, *Image Processing, Analysis and Machine Vision* (Chapman & Hall, London, 1993).
31. J. Hult, "Development of time resolved laser imaging techniques for studies of turbulent reacting flows," Ph.D. thesis (Lund Institute of Technology, Lund, Sweden, 2002).
32. M. Andersson, "Three-dimensional visualization of turbulent flames using shape-based interpolation," Master's thesis (Lund Institute of Technology, Lund, Sweden, 2000).
33. J. Hult, G. Josefsson, M. Aldén, and C. F. Kaminski, "Flame front tracking and simultaneous flow field visualisation in turbulent combustion," presented at the 10th International Symposium on Applications of Laser Techniques to Fluid Mechanics, Lisbon, Portugal, 10–13 July 2000.
34. H. Malm, G. Sparr, J. Hult, and C. F. Kaminski, "Nonlinear diffusion filtering of images obtained by planar laser-induced fluorescence spectroscopy," J. Opt. Soc. Am. A **17,** 2148–2156 (2000).